INTERNATIONAL JOURNAL OF CLIMATOLOGY
Int. J. Climatol. (2017)
Published online in Wiley Online Library
(wileyonlinelibrary.com) DOI: 10.1002/joc.5313

RMetS
Royal Meteorological Society

Different influences on the tropical Pacific SST gradient from natural and anthropogenic forcing

Liang Ning,[a,b,c] Jian Liu,[a,b]* Zhiyuan Wang[a,b] and Raymond S. Bradley[c]

[a] *Key Laboratory of Virtual Geographic Environment, Ministry of Education, State Key Laboratory of Geographical Environment Evolution, Jiangsu Provincial Cultivation Base, School of Geographical Science, Nanjing Normal University, China*

[b] *Jiangsu Center for Collaborative Innovation in Geographical Information Resource Development and Application, Nanjing Normal University, Nanjing, China*

[c] *Climate System Research Center, Department of Geosciences, University of Massachusetts, Amherst, MA, USA*

ABSTRACT: The influences of natural forcings (i.e. solar radiation and volcanic aerosol) and anthropogenic forcings (i.e. greenhouse gases) on the tropical Pacific zonal sea-surface temperature (SST) gradient are investigated through numerical sensitivity experiments, forced by natural forcing, anthropogenic forcing, or full forcing (both natural and anthropogenic forcing) using the Community Earth System Model (CESM) over the past two millennia. Under full forcing, during the present warming period (PWP; 1901–1999), the Pacific SST shows a larger warming over the tropical Pacific region than the subtropical Pacific region. This pattern is composed of an El Niño-like SST gradient (due to the greenhouse gas forcing) and a La Niña-like SST gradient (due to natural forcing). Two sensitivity experiments, the PWP under greenhouse gas forcing and the medieval warming period (MWP; 751–1250) under natural forcing, were used to examine the mechanisms. The results showed that under the greenhouse gas forcing, the larger warming over the eastern tropical Pacific is induced by an increased surface net heat flux, which is mainly caused by short-wave radiation and long-wave radiation. Under natural forcing, a larger warming is induced over the western tropical Pacific by changes in the ocean vertical heat transportation, caused by surface wind anomalies.

KEY WORDS natural forcing; anthropogenic forcing; tropical Pacific SST gradient

Received 4 May 2016; Revised 2 August 2017; Accepted 5 September 2017

1. Introduction

The Intergovernmental Panel on Climate Change (IPCC) Fourth Assessment Report (AR4) and Fifth Assessment Report (AR5) indicate that the global mean surface temperature increased by approximately 0.74 °C over the past century (Trenberth *et al.*, 2007; Hartmann *et al.*, 2013) with intensified climate extreme events (Easterling *et al.*, 2000a, 2000b). Based on the general circulation model (GCMs) simulations from the Coupled Model Intercomparison Project Phase 5 (CMIP5), by the end of the 21st century, this warming will reach 1–4 °C (relative to 1986–2005), depending on various emission scenarios (Collins *et al.*, 2013).

Among the different aspects of climate change, the response of the tropical Pacific to increased greenhouse gases (GHGs) has attracted much attention (Diaz and Markgraf, 2000; DiNezio *et al.*, 2009) because the tropical Pacific sea-surface temperatures (SST) strongly influence regional climates, as shown in both observational data (Diaz and Kiladis, 1992; Kunkel and Angel, 1999; Bradbury *et al.*, 2002; Ning and Bradley, 2014, 2015a, 2015b) and model simulations (Yu *et al.*, 2012; Weare, 2013; Zou *et al.*, 2014). The spread of the predicted changes in the tropical Pacific SST in the AR5 model simulations also determines the uncertainty of the projections of both monsoons (He and Zhou, 2015) and the western Pacific subtropical high (Chen and Zhou, 2015).

Future changes in the tropical Pacific SST, including its mean state (i.e. the zonal SST gradient) and variability (e.g. El Niño events), are still under debate (Knutson and Manabe, 1995; Clement *et al.*, 1996; Meehl *et al.*, 2000; Van Oldenborgh *et al.*, 2005; Guilyardi *et al.*, 2009; Collins *et al.*, 2010; Guilyardi *et al.*, 2012). For the mean state of tropical Pacific SST, there are different feedbacks involved in the time-mean response of the tropical Pacific climate system to greenhouse warming (Timmermann *et al.*, 1999; Diaz *et al.*, 2001). On the one hand, multi-model ensembles project a weak shift towards conditions that may be described as an El Niño-like state, with SSTs over the eastern and central equatorial Pacific warming more than those over the west, a state that is associated with weaker tropical circulation, in response to the increase of GHGs (Meehl *et al.*, 2007). This El Niño-like change can be attributed to the cloud-albedo feedback (Meehl and Washington, 1996) over the western tropical Pacific, or the slow-down of the Walker circulation induced by the increased moist static energy in the atmosphere being greater than the energy

* Correspondence to: J. Liu, Jiangsu, #1 Wenyuan Road, Qixia District, School of Geographical Science, Nanjing Normal University, Nanjing 210023, China. E-mail: jliu@njnu.edu.cn

transport associated with precipitation (Held and Soden, 2006; Vecchi *et al.*, 2006). On the other hand, the 'dynamical thermostat' mechanism indicates that a strong equatorial upwelling in the eastern tropical Pacific will weaken the warming over this region and induce stronger warming over the western tropical Pacific, creating a La Niña-like state (Cane *et al.*, 1997). This mechanism is supported by paleoclimate proxy data from the past millennium (Cobb *et al.*, 2003; Mann *et al.*, 2005). As an important component of the Bjerknes feedback (Bjerknes, 1969), ocean dynamics (Chang *et al.*, 2005) play very important roles in both of the equatorial Pacific SST warming states, especially over the cold tongue, where vertical ocean heat transport dominates the sea surface heat budget (Seager *et al.*, 1988). In response to a weaker Walker circulation, the ocean surface currents and vertical upwelling over the cold-tongue are reduced, and combined with an increased thermal stratification, the increased cooling by ocean vertical heat transport balances the warming over the cold tongue (DiNezio *et al.*, 2009; Xie *et al.*, 2010). However, in the 'dynamical thermostat' mechanism, the enhanced Walker circulation increases ocean upwelling and causes the thermocline to shoal in the east; both ocean dynamical responses induce smaller warmings over the eastern tropical Pacific and further strengthen the equatorial SST gradient (Clement *et al.*, 1996; Seager and Murtugudde, 1997). Meanwhile, the different signs of the tropical Pacific SST gradient changes and tropical atmospheric circulations found in different observational data sets (Cane *et al.*, 1997; Hansen *et al.*, 2006; Zhang and Song, 2006; Vecchi *et al.*, 2008) make this issue more complicated.

To improve projections of the future tropical Pacific SST mean state changes, the contributions from different dynamical and thermodynamical mechanisms, including these opposite feedbacks, under future warming should be evaluated. Recently, through several long-term model simulations, Liu *et al.* (2013) found that the warming due to solar radiation leads to a stronger SST gradient over the tropical Pacific, whereas the warming due to GHGs leads to a reduced one, demonstrating that both an El Niño-like state and a La Niña-like state have their own realms of validity. This finding also illustrates the need to differentiate the influences from natural forcing (e.g. solar radiation and volcanic aerosols) and anthropogenic forcing (e.g. GHGs emissions) when analysing the tropical Pacific SST mean state changes.

Most previous studies (e.g. DiNezio *et al.*, 2009; Xie *et al.*, 2010) mainly focused on the responses of the tropical Pacific SST gradient to increased anthropogenic GHGs emissions. Only a few studies (e.g. Liu *et al.*, 2013) examined the influences of natural forcings on the tropical Pacific SST gradient changes. Therefore, in this study, we used the Community Earth System Model (CESM) to run two 2000-year sensitivity simulations driven by (1) natural forcing, (2) GHGs emissions and (3) a 2000-year simulation driven by full forcing (both natural forcing and anthropogenic forcing) to quantitatively analyse the influence of natural forcing and anthropogenic forcing on tropical Pacific SST gradient changes.

2. Data and methodology

2.1. Experimental design

Three sensitivity experiments were performed using the National Center for Atmospheric Research (NCAR) Community Earth System Model (Gent *et al.*, 2011; Neale *et al.*, 2013) under full forcing (i.e. both natural forcing and anthropogenic forcing), natural forcing (i.e. solar radiation and volcanic eruptions) and anthropogenic forcing (i.e. GHG emissions) over the period 1–2000 AD. The atmospheric component used here is the Community Atmosphere Model version 4 (CAM4) with a horizontal resolution of $3.75 \times 3.75^{\circ}$ and 26 vertical levels. The ocean component used here is the Parallel Ocean Program (POP) version 2, with 116 grids in latitude by 100 grids in longitude and 60 vertical levels.

The full forcing run is externally forced by the orbital parameters, solar variability, stratospheric volcanic aerosols, land use and land cover changes and well-mixed GHG concentrations in the atmosphere (including CO_2, CH_4 and N_2O and other trace gases). The solar radiation forcing used in this study is reconstructed using cosmogonic isotopes ^{10}Be in ice cores, ranging about 1360–1370 W m^{-2} (Shapiro *et al.*, 2011). The volcanic aerosol forcing is defined as global volcanic sulphate aerosol masses injection reconstructed using a comprehensive set of ice cores, ranging 0–0.015 kg m^{-2} (Gao *et al.*, 2008). The concentrations of GHGs over the industrial period are taken from the Goddard Institute for Space Studies, and the values are then linked with splines through the ice core results over the last two millennia, increasing from 275 to 370 ppm for CO_2, from 700 to 1700 ppb for CH_4 and from 270 to 310 ppb for N_2O (MacFarling Meure *et al.*, 2006). The time series of the individual forcings used in the CESM simulations are shown in Wang *et al.* (2015, figure 1), and more details can be found in the corresponding description.

2.2. Data

The SST gradient calculated from the observed Hadley Centre Sea Ice and Sea Surface Temperature data set (HadISST) during the present warming period (PWP; 1901–2000) is first used to validate the model's performance in reproducing the tropical Pacific SST gradient. The simulated SSTs over the tropical Pacific region are used to examine the changes in SST gradient during different typical warming periods, that is, the PWP (1901–2000) under the full forcing and GHGs forcing experiment and the medieval warming period (MWP, 751–1250) under the natural forcing experiment, with respect to the pre-industrial period (1–1850) as a reference period. When analysing the mechanisms behind the SST gradient changes, the net surface heat flux and the surface short-wave radiation flux, long-wave radiation flux, latent heat flux and sensible heat flux from each sensitivity experiment were used to examine the surface heat budget. Then, the surface wind field and shallow ocean vertical heat transport (0–30 m) were used to examine the dynamic influence on the SST gradient changes.

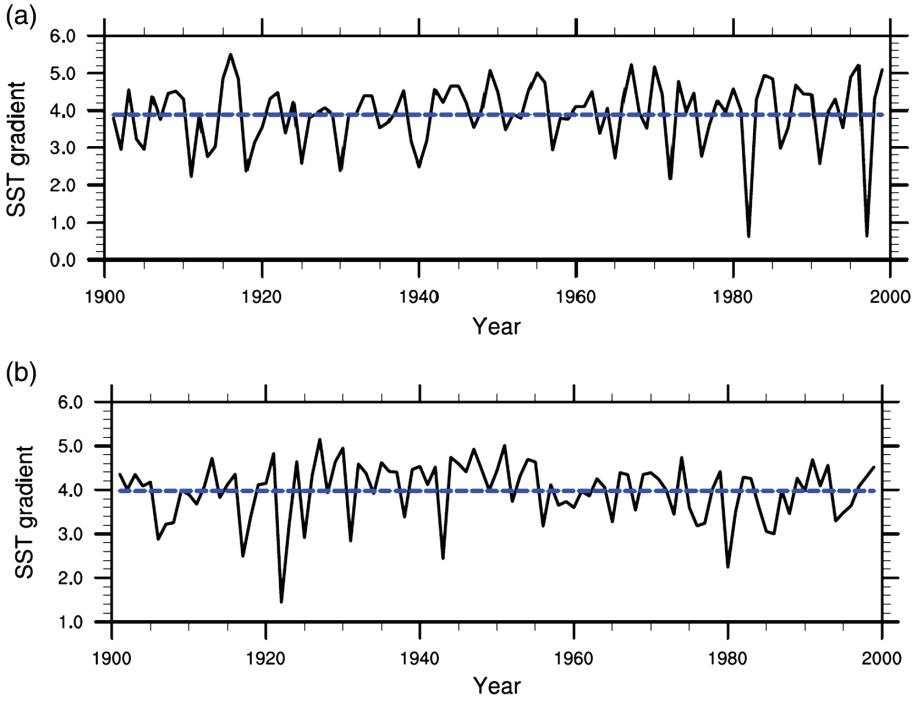

Figure 1. The observed (a) and simulated (b) tropical Pacific SST gradient time series (black solid lines) are defined as the difference between the SST averages over the region (−5° to 5°N, 150°−170°E) and the region (−5° to 5°N, −120° to −100°E) over the past 100 years (unit: °C). The simulated result is from the experiment driven by all forcings. The dashed lines indicate the averages of the SST gradients. [Colour figure can be viewed at wileyonlinelibrary.com].

3. Results

3.1. Comparison between observed and simulated tropical Pacific SST gradients during the PWP

Figure 1 compares the observed and simulated tropical Pacific SST gradient time series defined as the difference between the SST averages over the warm pool (−5° to 5°N, 150°−170°E) and the cold tongue (−5° to 5°N, −120° to −100°E) during the PWP. Both the observed and simulated SST gradients have averages of approximately 4 °C, with their smallest values at approximately 1 °C, indicating that the model can reproduce both the average SST gradient and the variability, especially for strong El Niño events with magnitudes similar to those seen in the observations.

3.2. The mechanisms behind the tropical Pacific SST gradient changes based on a full forcing experiment

During the PWP, under full forcing, the tropical Pacific SST change shows a pattern of enhanced warming relative to the subtropics (Figure 2(a)), indicating a more robust response of the equatorial Pacific than was found in previous studies (e.g. Liu *et al.*, 2005).

3.2.1. Changes in surface heat fluxes

Figure 2(b) shows that the surface net heat flux (∼5 W m^{-2}) is a major forcing that enhances the equatorial warming over the eastern and central tropical Pacific, but not over the western tropical Pacific. Positive values indicate the ocean receives energy. There are significant increases over the eastern and central equatorial Pacific but decreases over the western equatorial Pacific and subtropical Pacific. This pattern is mainly caused by the changes in the short-wave radiation (Figure 3(a)) and latent heat flux (Figure 3(c)) and is partially caused by the changes in the sensible heat flux (Figure 3(d)), though by smaller amounts (∼1 W m^{-2}). In comparison, the long-wave heat flux changes are uniform over the whole region (Figure 3(b)), but have a smaller magnitude (∼2 W m^{-2}), while the larger increases are located over the regions with surface net heat flux decreases (i.e. the western equatorial Pacific and subtropical Pacific).

Over the eastern and central tropical Pacific, the short-wave radiation increased (Figure 3(a)) because of decreased low cloud cover and middle cloud cover (Figures S1(a) and (b), Supporting Information). Over the western tropical Pacific, the short-wave radiation is reduced because of increased middle cloud cover (Figure S1(b)), while over the subtropical Pacific, the short-wave radiation is reduced because of increased low and middle cloud cover (Figures S1(a) and (b)). These increased low and middle cloud covers (caused by the increased mean stability) reduce the incoming short-wave radiation over the sea surface. The increased long-wave radiation over the western equatorial Pacific and subtropical Pacific (Figure 4(b)) is mainly due to the increased high cloud cover, which traps the outgoing long-wave radiation emitted by the earth and radiates it downwards (Figure S1(c)).

The changes in the latent heat flux (Figure 3(c)) are determined by the changes in two factors, that is, the

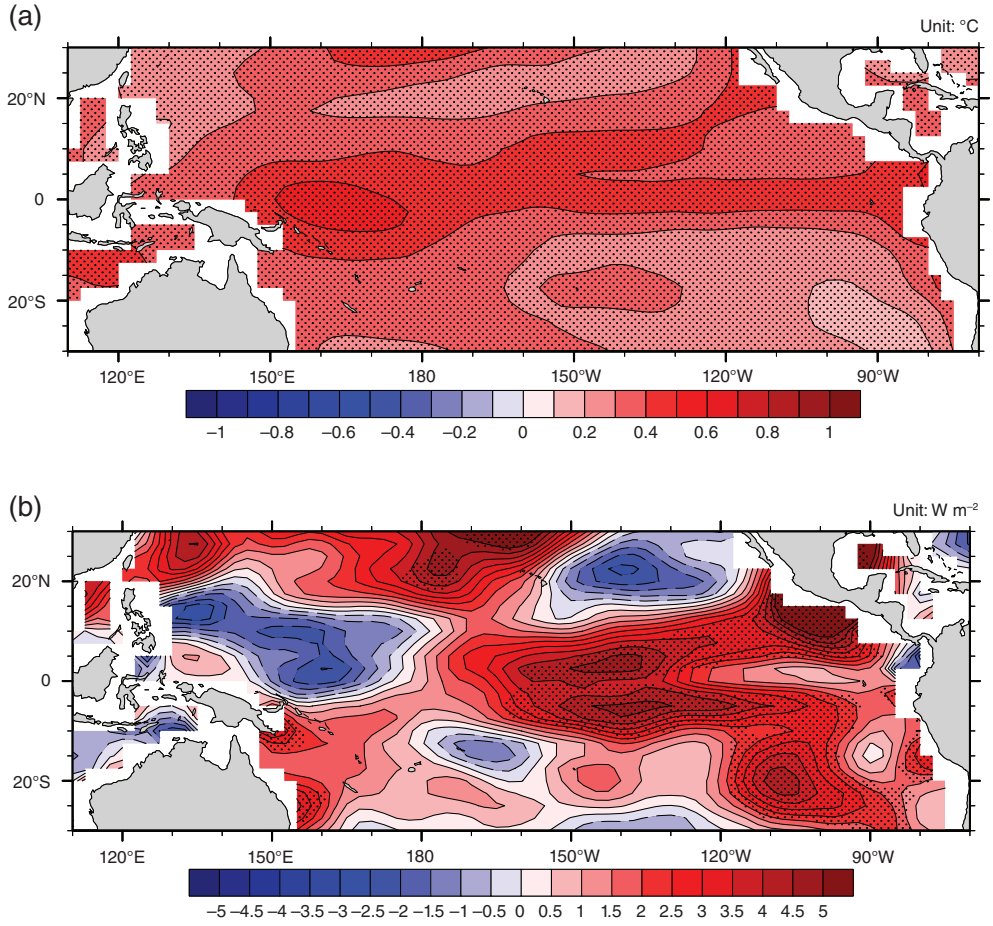

Figure 2. The simulated tropical Pacific SST changes (a, unit: °C) and the net surface heat flux changes (b, unit: W m^{-2}) from the all-forcing experiment over the PWP (1901–2000) compared to the relevant pre-industrial period (1–1850). Positive values are into the ocean. Stippling indicates that the changes are significant at the $p = 0.05$ level based on the Student's t-test.

wind velocity and the differences between the surface saturation-specific humidity and actual surface-specific humidity (Fu *et al.*, 1992). Because the surface air temperature increases more than the SST during the PWP, the surface saturation-specific humidity increases more than the actual surface-specific humidity (Knutson and Manabe, 1995), inducing a decreased latent heat flux over the whole region. However, over the eastern and western equatorial Pacific, due to the reduction of the surface wind (which reflects a reduced Walker circulation) (Figure 4), there are positive latent heat flux anomalies, which means ocean latent heat loss is reduced. For the subtropical Pacific, because of the increases in both the specific humidity difference and wind speed, there are significantly negative latent heat flux anomalies (enhanced latent heat flux). Therefore, this spatial pattern of latent heat flux changes contributes to the enhanced SST increases over the equatorial Pacific. Similarly, due to the surface air temperature increases being larger than SST increases, there are positive sensible heat flux changes over the whole region, especially over the eastern tropical Pacific (Figure 3(d)), but the magnitudes of the sensible heat flux changes are smaller than the other heat flux changes.

3.2.2. *Changes in atmospheric circulation*

The changes in the surface wind field during the PWP show a weakened zonal wind over the eastern equatorial Pacific but an enhanced zonal wind over the western equatorial Pacific (Figure 4). This pattern is different from the weakening of the Walker circulation over the whole equatorial Pacific simulated in previous studies (e.g. Xie *et al.*, 2010), indicating that there are other mechanisms involved besides the well-known responses of the global mean precipitation and atmospheric humidity to global warming (Held and Soden, 2006; Vecchi and Soden, 2007). Similar patterns were also found in a 26-model ensemble from CMIP5, showing the strengthening and westwards-shifting trend of the Pacific Walker circulation in response to the recent La Niña-like anomalous SST forcing (Ma and Zhou, 2016).

3.2.3. *Ocean dynamical responses and corresponding changes in the ocean heat transport*

In response to the weaker Walker circulation over the eastern equatorial Pacific, the ocean upwelling in the top 30 m is reduced (Figure 5(a)). However, over the western equatorial Pacific, the enhanced zonal winds induced a

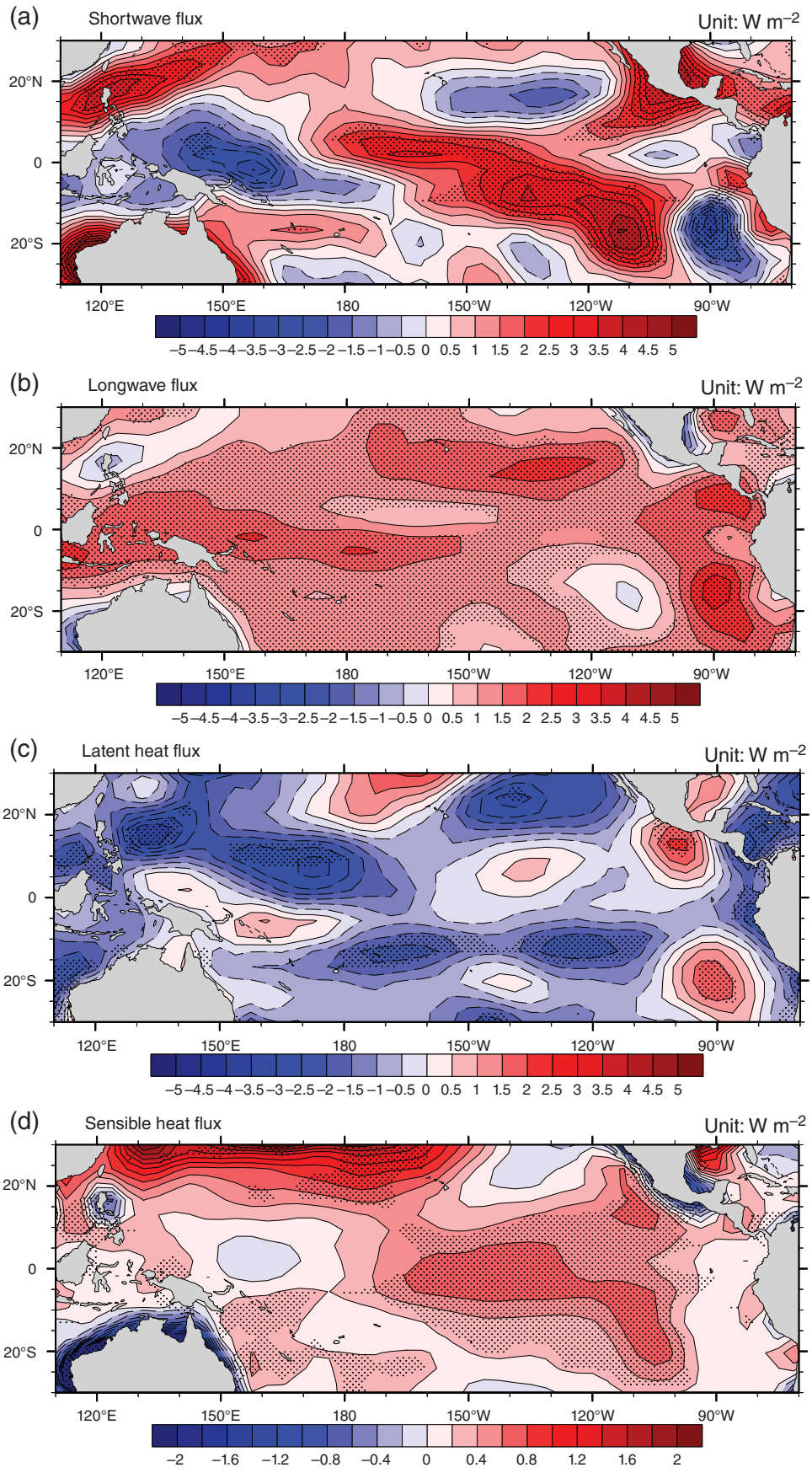

Figure 3. The simulated surface short-wave radiation flux changes (a, unit: W m^{-2}), long-wave radiation flux changes (b, unit: W m^{-2}), latent heat flux changes (c, unit: W m^{-2}) and sensible heat flux changes (d, unit: W m^{-2}) from the all-forcing experiment over the PWP (1901–2000) compared to the relevant pre-industrial period (1–1850). Positive values are into the ocean.

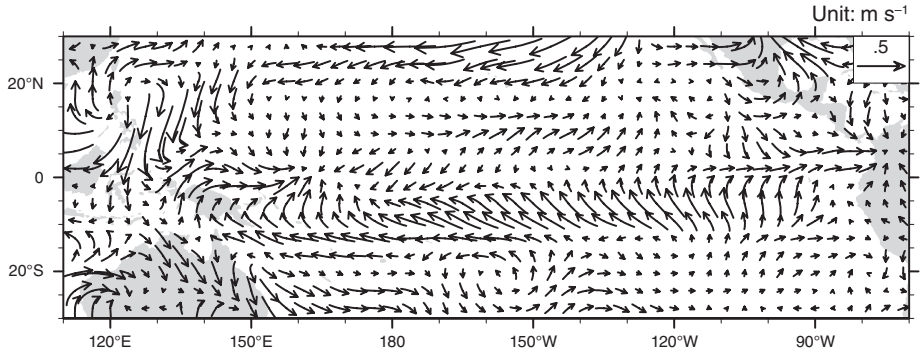

Figure 4. The simulated surface wind changes (unit: $m\,s^{-1}$) from the all-forcing experiment over the PWP (1901–2000) pre-industrial period (1–1850).

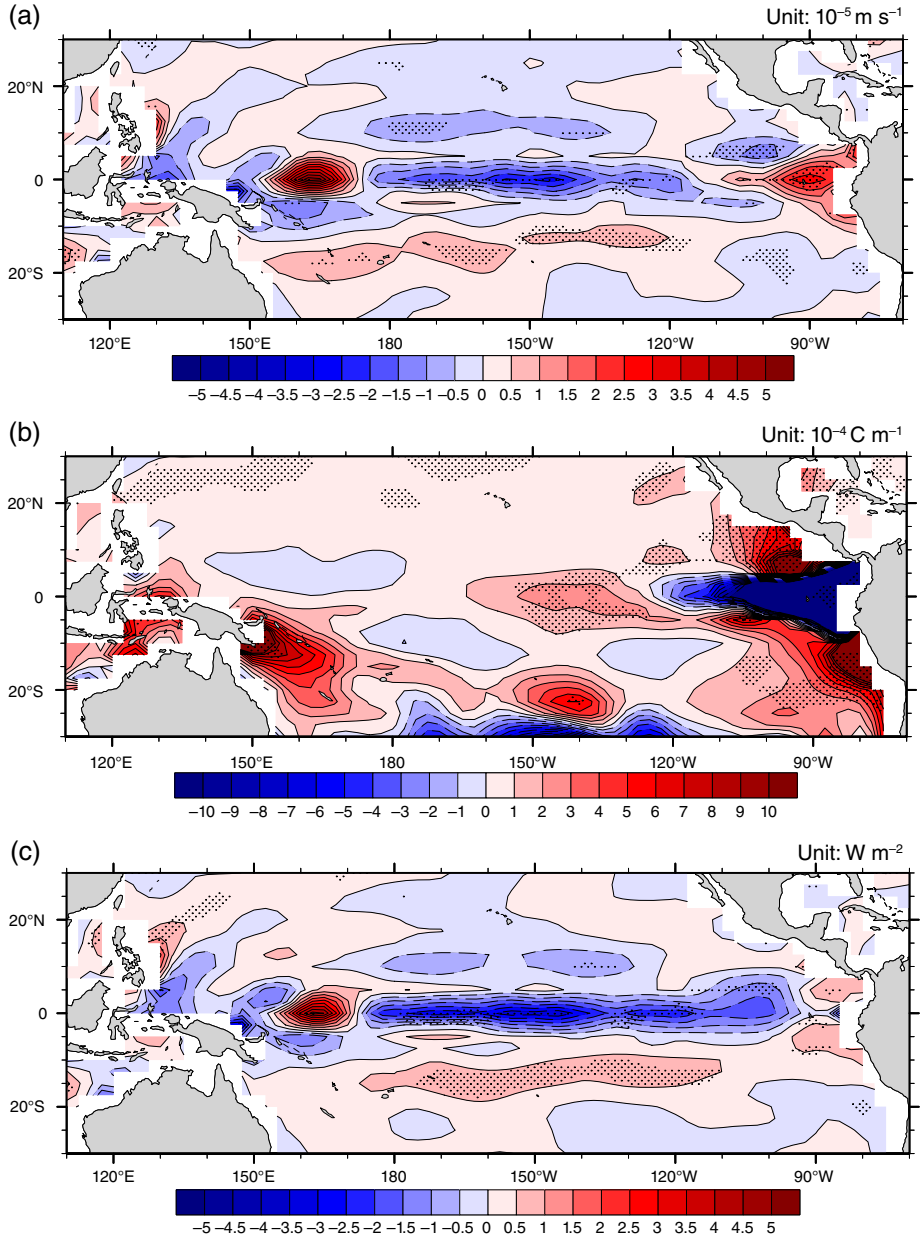

Figure 5. The simulated ocean vertical velocity changes (a, unit: $10^{-5}\,m\,s^{-1}$; positive upwards), vertical temperature gradient (b, unit: $10^{-4}\,°C\,m^{-1}$) and vertical heat transportation changes (c, unit: $W\,m^{-2}$; positive values are in the surface layer of the ocean) from the all-forcing experiment over the PWP (1901–2000) with relevant to pre-industrial period (1–1850). [Colour figure can be viewed at wileyonlinelibrary.com].

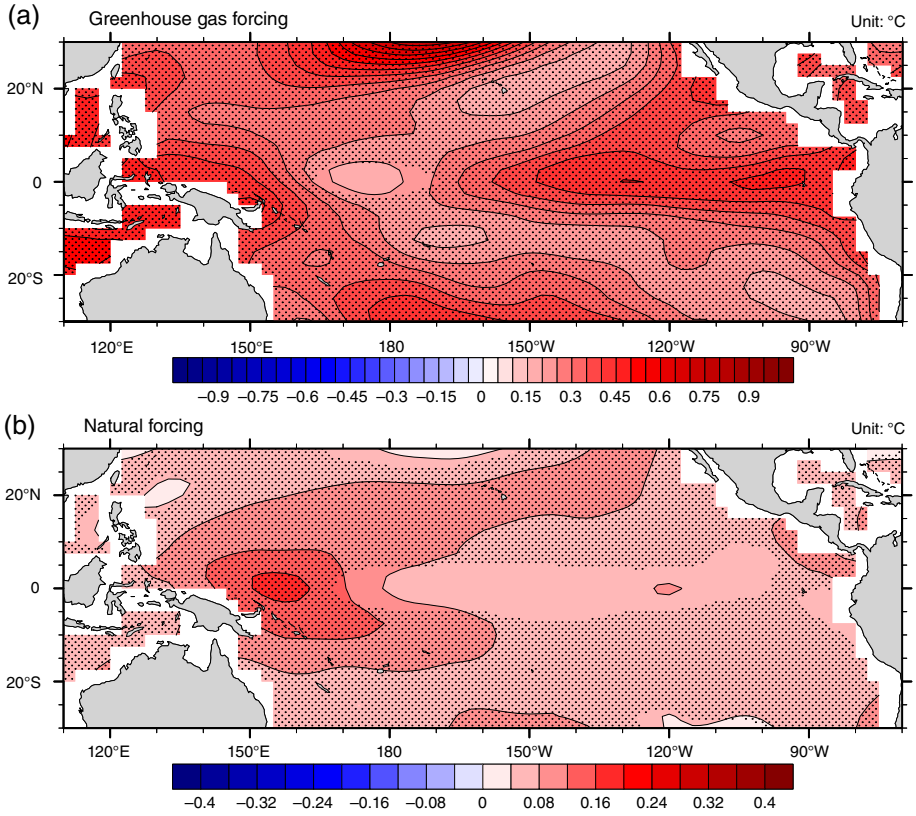

Figure 6. The simulated tropical Pacific SST changes (unit: °C) from the GHGs sensitivity experiment (a) over the PWP (1901–2000) with relevant to pre-industrial period (1–1850) and from natural forcing sensitivity experiment (b) over the MWP (751–1250) with relevant to pre-industrial period (1–1850). Stippling indicates that the changes are significant at the $p = 0.05$ level based on the Student's t-test. [Colour figure can be viewed at wileyonlinelibrary.com].

positive ocean vertical velocity (Figure 5(a)). The ocean thermodynamical response shows a nearly uniform pattern of an increased vertical temperature gradient, with the most significant increases over the eastern to central equatorial Pacific (Figure 5(b)).

Both the dynamical responses and thermodynamical responses of the ocean result in a negative ocean vertical heat transport over the eastern equatorial Pacific but a positive ocean vertical heat transport over the western equatorial Pacific (Figure 5(c)). The ocean vertical heat transport (Q_w) here is defined following DiNezio *et al.* (2009):

$$Q_w = -\rho_0 c_p \int_{-H}^{0} w \frac{\partial T}{\partial z} dz \qquad (1)$$

where ρ_0 is the ocean water density, c_p is the ocean heat capacity, w is the vertical velocity of ocean water, T is the ocean temperature, z is the depth of the ocean water and H is chosen as 30 m.

Therefore, the enhanced equatorial warming during the PWP under full forcing is not the same as that seen in previous model simulations, which shows that the surface heat flux is a major forcing for the warming over the whole equatorial Pacific (e.g. Liu *et al.*, 2005). The enhanced warming over the equatorial Pacific in our current study is composed of two parts: the warming over the cold tongue induced by the surface heat flux changes and the warming over the warm pool induced by the zonal wind changes. These mechanisms will be examined in detail through two sensitivity experiments shown in the following section.

3.3. Tropical Pacific SST gradient changes based on GHG forcing and natural forcing experiments and their corresponding mechanisms

The SST changes during PWP under the GHG forcing (Figure 6(a)) and during the MWP under natural forcing (Figure 6(b)) showed opposite spatial characters: the maximum SST changes during the PWP (~0.6 °C) are located over the eastern tropical Pacific, while the maximum SST changes during the MWP (~0.2 °C) are located over the western tropical Pacific. The spatial patterns are similar to the SST anomaly distributions during El Niño events and La Niña events, respectively, but on a much longer time scale. This comparison can also explain the enhanced tropical Pacific warming under full forcing (Figure 2(a)), which is composed of these two spatial patterns.

3.3.1. Changes in the surface heat fluxes

For the GHG forcing sensitivity experiment, the distribution of the net surface heat flux changes shows significant increases over the eastern tropical Pacific and

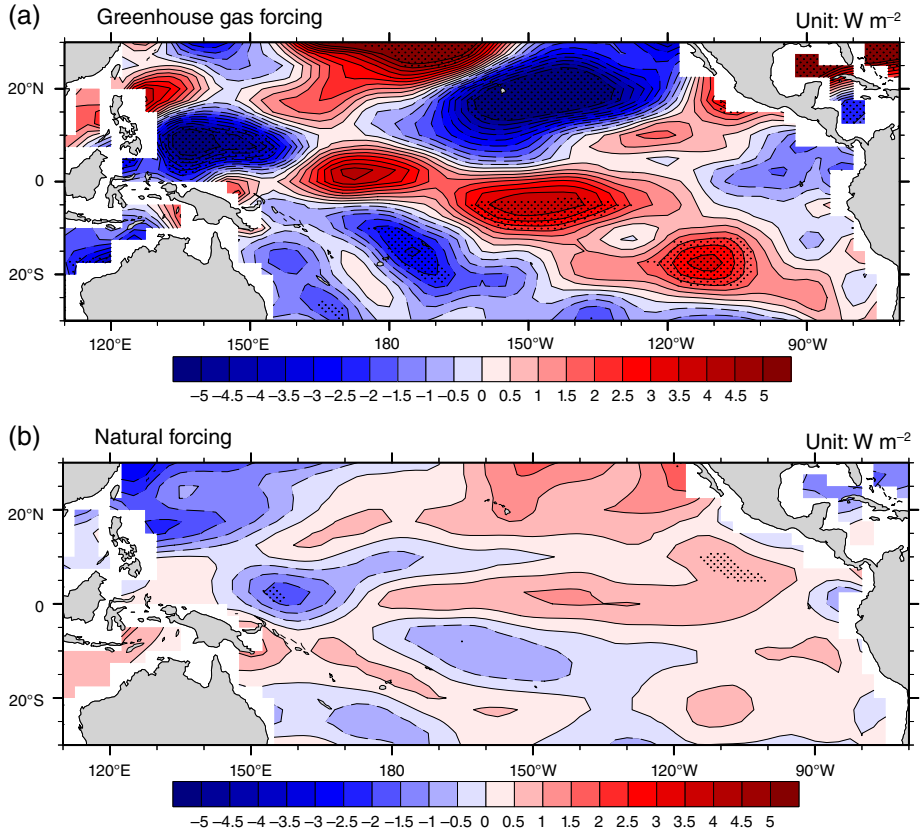

Figure 7. The simulated net surface heat flux changes (unit: W m^{-2}) from the GHGs sensitivity experiment (a) over the PWP (1901–2000) with relevant to pre-industrial period (1–1850) and from the natural forcing sensitivity experiment (b) over the MWP (751–1250) with relevant to pre-industrial period (1–1850). [Colour figure can be viewed at wileyonlinelibrary.com].

significant decreases over the subtropical Pacific (Figure 7(a)). Although the heat flux increases extend to the western tropical Pacific, the increases over the dateline region are not significant.

The spatial patterns of the SST changes (Figure 6(a)) and net surface heat flux changes under GHG forcing (Figure 7(a)) can be explained by a larger increase in the short-wave radiation (Figure S2(a)) and long-wave radiation (Figure S2(b)) over the eastern tropical Pacific region and a larger decrease in the latent heat flux over the subtropical region (Figure S2(c)). Under the GHG forcing, the latent heat loss is increased over the subtropical region but decreased over the equatorial Pacific region (Figure S2(c)). The increased latent heat loss (negative anomalies) over the subtropical region is caused by the increased trade winds and the difference between the surface saturation-specific humidity and the surface air-specific humidity, while the decreased latent heat loss (positive anomalies) over the tropical region is due to the decreased wind speed. The mechanism causing the higher sensitivity of the latent heat flux over the subtropics than that of the tropics is attributed to the stronger observed mean trade wind speed over the subtropics (Seager and Murtugudde, 1997). The increased sensible heat flux (Figure S2(d)) caused by the reduced temperature gradient between the sea surface and atmosphere can also contribute (~0.6 W m^{-2}) to the spatial pattern of the net surface heat flux changes.

For the MWP, which appears mainly under natural forcing (Liu *et al.*, 2013), the tropical Pacific SST gradient changes show a La Niña-like condition (Figure 6(b)). However, the corresponding net surface heat flux changes show non-significant changes over most of the region, with magnitudes within ±2 W m^{-2} (Figure 7(b)). There are positive changes over the eastern tropical Pacific and negative changes over the western tropical Pacific, with significant decreases over a small area. Therefore, this La Niña-like SST change pattern does not result from net surface heat flux changes, which should induce El Niño-like SST changes.

For this pattern of net surface heat flux changes, there are positive short-wave radiation flux changes (Figure S3(a)) over most of the tropical Pacific (1 W m^{-2}), except for over the western part of the warm pool (−1 W m^{-2}), because solar radiation is the major forcing anomaly in the MWP. The distribution of the long-wave radiation flux changes (Figure S3(b)) shows small but uniform increases over the whole tropical Pacific (0–0.5 W m^{-2}). The latent heat loss is enhanced (negative anomalies) over the equatorial tropical Pacific (Figure S3(c)), especially over the warm pool (−0.5 W m^{-2}), while the contributions from the sensible heat flux (Figure S3(d)) changes are smaller (−0.2 to 0.2 W m^{-2}).

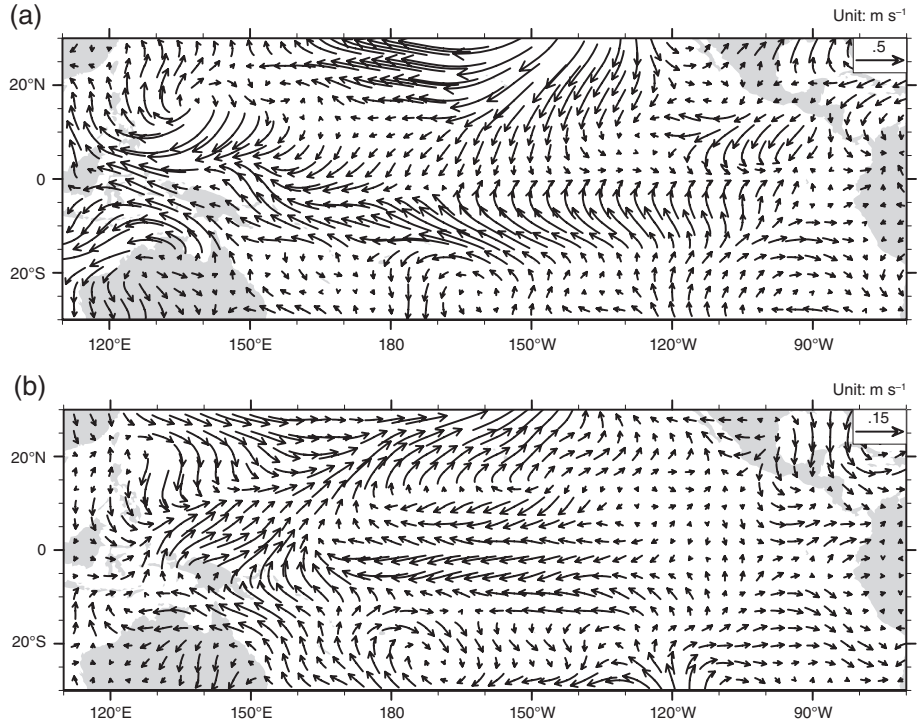

Figure 8. The simulated surface wind changes (unit: $m\,s^{-1}$) from the GHGs sensitivity experiment (a) over the PWP (1901–2000) with relevant to pre-industrial period (1–1850) and from the natural forcing sensitivity experiment (b) over the MWP (751–1250) with relevant to pre-industrial period (1–1850).

3.3.2. Changes in atmospheric circulation

Under GHG forcing, for the wind field anomalies, the increased GHGs induce westerly wind anomalies over the eastern tropical Pacific, indicating a slow-down of the Walker circulation (Figure 8(a)) under the external forcing (Vecchi and Soden, 2007). Over the western tropical Pacific, there are easterly wind anomalies, which is different from the previous pattern of a weaker Walker circulation over the whole tropical Pacific. The potential reason for this difference is that the increase of the GHG concentrations in the current study follows the observed CO_2 concentrations (from 280 to 375 ppm during PMP, cf. Wang *et al.*, 2015, figure 1(a)), which are smaller than those in the $2\times CO_2$ or $4\times CO_2$ experiments (e.g. DiNezio *et al.*, 2009).

Under natural forcing, the spatial pattern of wind field anomalies is typical of La Niña-like conditions (with an enhanced Walker circulation) (Figure 8(b)), and the magnitudes are smaller than those under the GHG forcing.

3.3.3. Ocean dynamical response and corresponding changes in ocean heat transport

In the GHG forcing sensitivity experiment, the easterly wind anomalies reduce the upwelling over the cold-tongue (Figure 9(a)); however, due to the increase in the vertical temperature gradient (Figure 9(b)), the net changes in the vertical heat transportation are negative over the eastern and central tropical Pacific (Figure 9(c)). This is consistent with the previous conclusion that an enhanced equatorial warming is associated with surface latent heat flux, short-wave cloud forcing and surface ocean mixing, while an El Niño-like pattern response is associated with equatorial ocean upwelling and a wind-upwelling, dynamic ocean–atmosphere feedback (Liu *et al.*, 2005).

In the natural forcing sensitivity experiment, the westerly wind anomalies lead to eastwards anomalies extending from the warm pool (Figure 10(a)) that, when combined with the reduced vertical temperature gradient (Figure 10(b)), result in large warmings over the region of 150°–170°E. Moreover, the vertical heat transport changes show slight changes (within $\pm 0.5\,W\,m^{-2}$) over most of the region, with large increases ($\sim 2\,W\,m^{-2}$) over only the western tropical Pacific (Figure 10(c)). This explains why the SST warming under natural forcing during the MWP is located over the western tropical Pacific and has a much smaller magnitude (Figure 6).

4. Conclusions

Three numerical sensitivity experiments using CESM were used to quantitatively investigate the different influences of the natural and anthropogenic forcings over the tropical Pacific zonal SST gradient. Under the full forcing, the tropical Pacific SST shows an enhanced equatorial warming during the PWP. This enhanced equatorial warming is composed of a pattern with greater warming over the cold tongue (El Niño-like SST gradient) and a pattern with greater warming over the warm pool (La Niña-like SST gradient), and these two patterns are generated

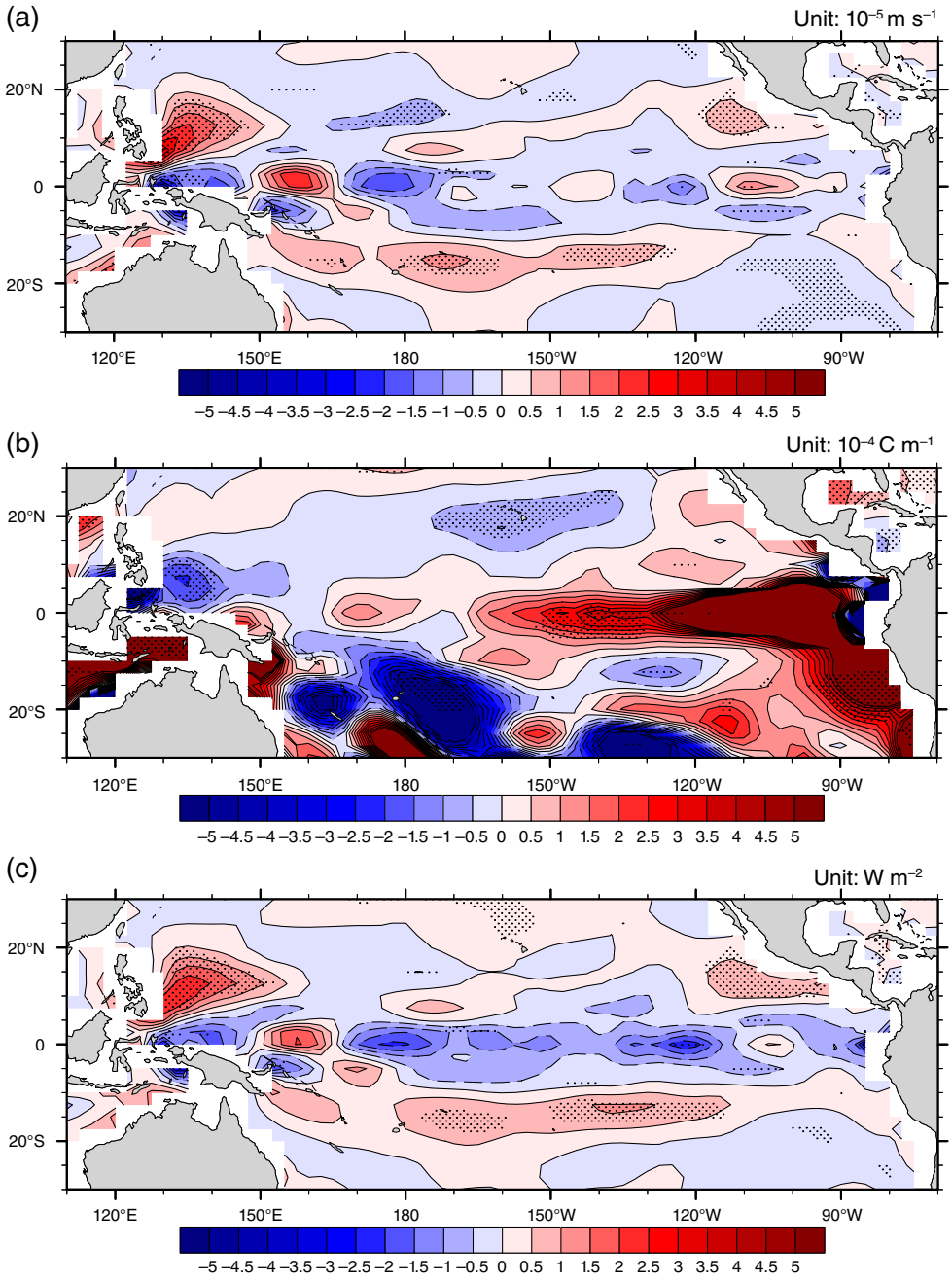

Figure 9. The simulated ocean vertical velocity changes (a, unit: 10^{-5} m s^{-1}; positive upwards), vertical temperature gradient (b, unit: 10^{-4} °C m^{-1}) and vertical heat transportation changes (c, unit: W m^{-2}; positive values are into the ocean surface layer) from the GHGs sensitivity experiment over the PWP (1901–2000) with relevant to pre-industrial period (1–1850). [Colour figure can be viewed at wileyonlinelibrary.com].

under the GHGs forcing and natural forcing separately. This enhanced equatorial warming is induced by the increased net surface flux over the cold tongue, which is related mainly to short-wave radiation and long-wave radiation, and positive changes in the ocean vertical heat transport due to the wind field anomalies over the warm pool.

These two mechanisms are then confirmed by sensitivity experiments with separated GHG and natural forcings. The evolutionary processes are summarized as following. Under the GHG forcing (Figure 11(a)), the uniform increase of long-wave radiation heats the atmosphere and increases moist static energy in the atmosphere. As a result, the Walker circulation slows down, and then the latent heat loss over the cold tongue reduces. Meanwhile, the reduced upwelling due to the slowdown of the Walker circulation, combined with the increased vertical ocean temperature gradient, result in a negative net changes in the vertical heat transportation over the eastern and central tropical Pacific. Moreover, cloud-albedo feedback makes the short-wave radiation increase larger over the cold tongue than over the warm pool. Therefore, an El Niño-like SST gradient change with greater warming over the cold-tongue is generated.

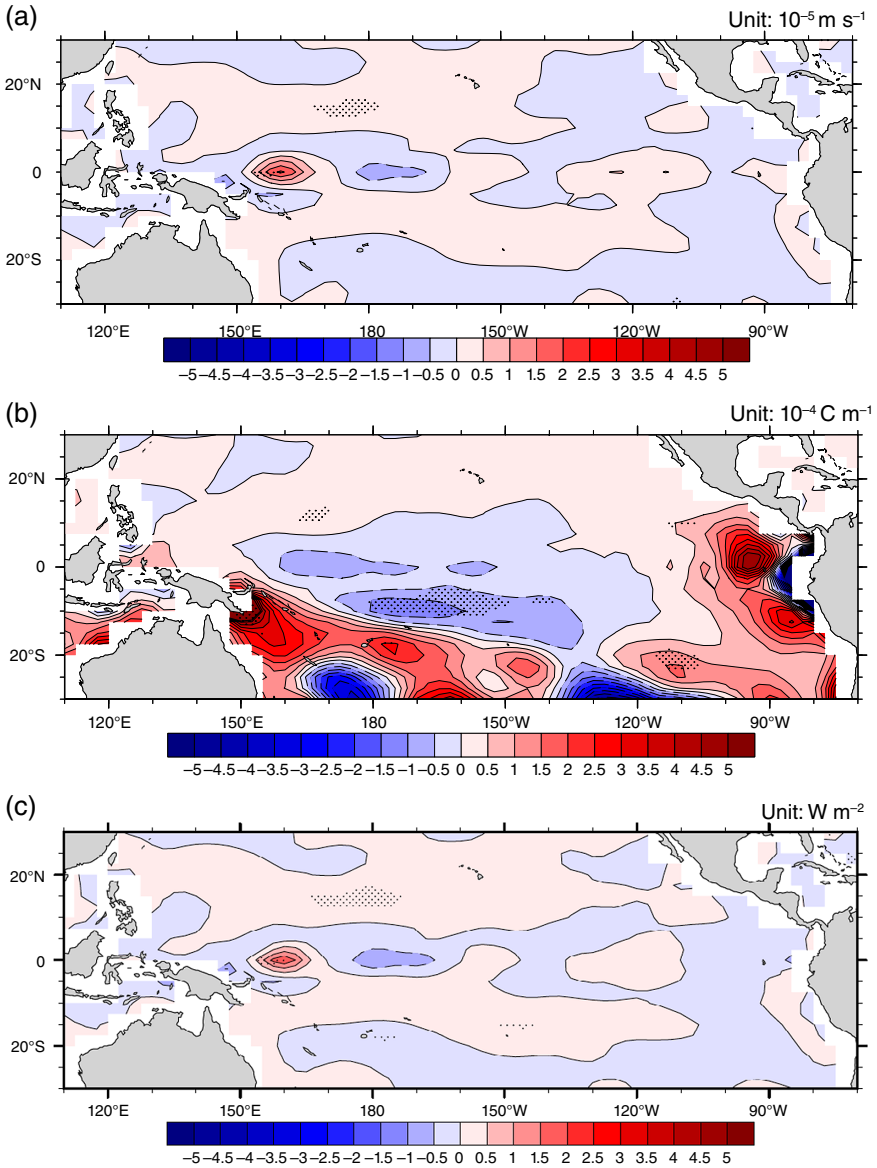

Figure 10. The simulated ocean vertical velocity changes (a, unit: 10^{-5} m s^{-1}; positive upwards), vertical temperature gradient (b, unit: 10^{-4} °C m^{-1}) and vertical heat transportation changes (c, unit: W m^{-2}; positive values are into the ocean surface layer) from natural forcing sensitivity experiment (c, d) over the MWP (751–1250) with relevant to pre-industrial period (1–1850). [Colour figure can be viewed at wileyonlinelibrary.com].

Under the natural forcing (Figure 11(b)), the increase of short-wave radiation directly heats the sea surface; however, the stronger upwelling partially offsets the warming over the cold tongue, resulting a larger SST gradient over the tropical Pacific. Therefore, the Walker circulation is enhanced through the Bjerknes feedback, and positive ocean vertical velocity anomalies and a decreased vertical temperature gradient, resulting in positive ocean vertical heat transport changes over the western tropical Pacific. Therefore, a La Niña-like SST gradient change with greater warming over the warm pool is generated, mainly through the mechanism similar to the dynamical thermostat mechanism originally defined by Clement *et al.* (1996). During these evolutionary responses, both fast response of the mixed layer warming at the time scale of several years and slow responses of deeper water upwelling changes and thermocline changes at longer time scale of tens to hundred years (Xie *et al.*, 2010) are involved, and their interactions establish the new SST patterns.

These results provide new insights into the controversial future changes in the zonal tropical Pacific SST gradient. Either an El Niño-like SST gradient change or a La Niña-like SST gradient change could be possible, depending on whether the GHG or natural forcing is more dominant in the future, but, given the trajectory of GHG emissions, the former seems to be the more likely scenario.

Acknowledgements

This research is jointly supported by the National Natural Science Foundation of China (grant nos. 41501210, 41371209 and 41420104002), the National Key

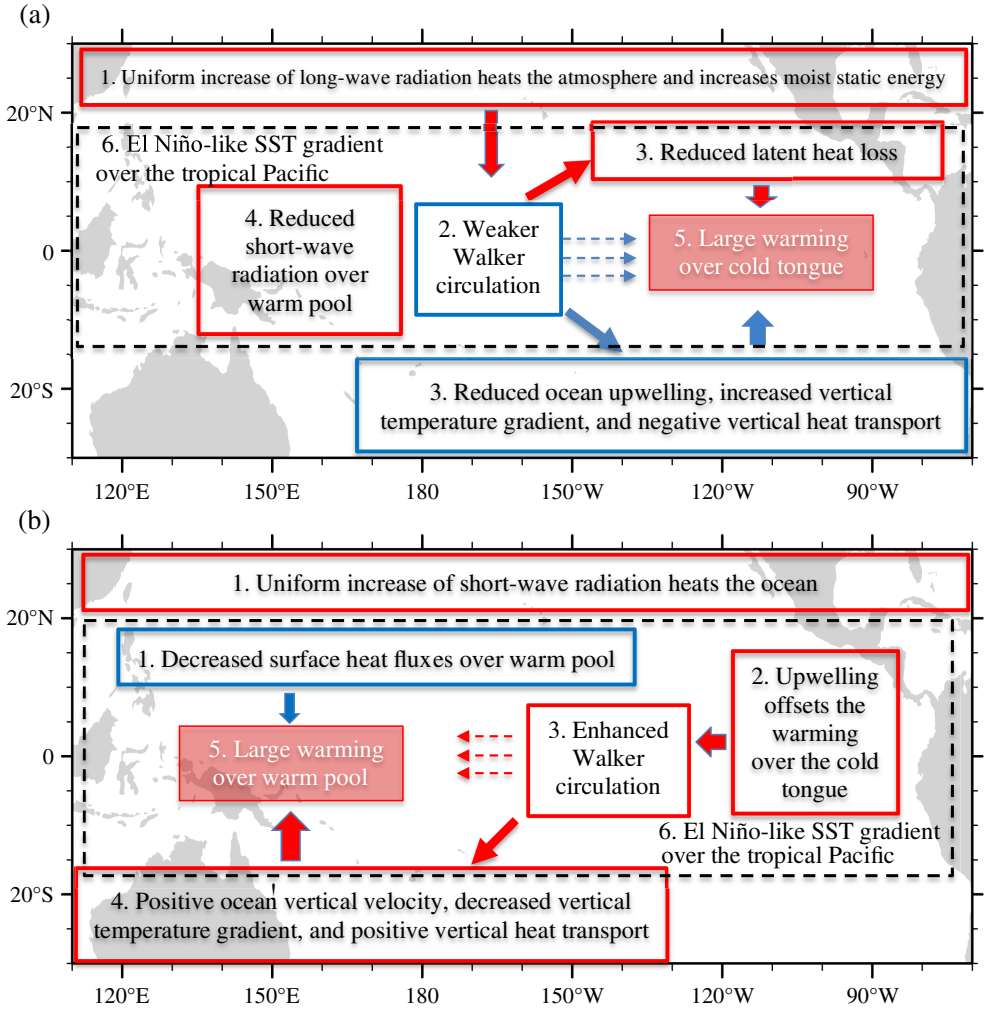

Figure 11. The schematic diagram of the mechanisms influencing the tropical Pacific SST gradient distributions from the GHG forcing sensitivity experiment (a) and natural forcing experiment (b). [Colour figure can be viewed at wileyonlinelibrary.com].

Research and Development Program of China (grant no. 2016YFA0600401), the Jiangsu Province Natural Science Foundation (grant no. BK20150977), National Natural Science Foundation of China (grant no. 41631175) and the Priority Academic Development Program of Jiangsu Higher Education Institutions (grant no. 164320H116). The Hadley Centre Sea Ice and Sea Surface Temperature data set (HadISST) were obtained from the Met Office.

Supporting information

The following supporting information is available as part of the online article:

Figure S1. The simulated low-level cloud cover changes (a, unit: %), middle-level cloud cover changes (b, unit: %) and high-level cloud cover changes (c, unit: %), from the all-forcing experiment over the PWP (1901–2000) with relevant to pre-industrial period (1–1850).

Figure S2. The simulated surface short-wave radiation flux changes (a, unit: $W\,m^{-2}$), long-wave radiation flux changes (b, unit: $W\,m^{-2}$), latent heat flux changes (c, unit: $W\,m^{-2}$) and sensible heat flux changes (d, unit: $W\,m^{-2}$) from the GHGs sensitivity experiment over the PWP (1901–2000) with relevant to pre-industrial period (1–1850). Positive values are into the ocean.

Figure S3. The simulated surface short-wave radiation flux changes (a, unit: $W\,m^{-2}$), long-wave radiation flux changes (b, unit: $W\,m^{-2}$), latent heat flux changes (c, unit: $W\,m^{2}$) and sensible heat flux changes (d, unit: $W\,m^{2}$) from the natural forcing sensitivity experiment over the MWP (751–1250) with relevant to pre-industrial period (1–1850). Positive values are into the ocean.

References

Bjerknes J. 1969. Atmospheric teleconnections from the equatorial Pacific. *Mon. Weather Rev.* **97**: 163–172.

Bradbury JA, Dingman SL, Keim BD. 2002. New England drought and relations with larger scale atmospheric circulation patterns. *J. Am. Water Resour. Assoc.* **38**: 1287–1299.

Cane MA, Clement AC, Kaplan A, Kushnir Y, Pozdnyakov D, Seager R, Zebiak SE, Murgugudde R. 1997. Twentieth-century sea surface temperature trends. *Science* **275**: 957–960.

Chang P, Yamagata T, Schopf P, Behera SK, Carton J, Kessler WS, Meyers G, Qu T, Schott F, Shetye S, Xie S-P. 2005. Climate fluctuations of tropical coupled systems – the role of ocean dynamics. *J. Clim.* **19**: 5122–5174.

Chen X, Zhou T. 2015. Distinct effects of global mean warming and regional sea surface warming pattern on projected uncertainty in the South Asian summer monsoon. *Geophys. Res. Lett.* **42**: 9433–9439. https://doi.org/10.1002/2015GL066384.

Clement AC, Seager R, Cane MA, Zebiak SE. 1996. An ocean dynamical thermostat. *J. Clim.* **9**: 2190–2196.

Cobb KM, Charles CD, Cheng H, Edwards RL. 2003. El Niño/Southern Oscillation and tropical Pacific climate during the last millennium. *Nature* **424**: 271–276.

Collins M, An S, Cai W, Ganachaud A, Guilyardi E, Jin FF, Jochum M, Lengaigne M, Power S, Timmermann A, Vecchi G, Wittenberg A. 2010. The impact of global warming on the tropical Pacific Ocean and El Niño. *Nat. Geosci.* **3**: 391–397.

Collins M, Knutti R, Arblaster J, Dufresne J-L, Fichefet T, Friedlingstein P, Gao X, Gutowski WJ, Johns T, Krinner G, Shongwe M, Tebaldi C, Weaver AJ, Wehner M. 2013. Long-term climate change: projections, commitments and irreversibility. In *Climate Change 2013: The Physical Science Basis. Contribution of Working Group I to the Fifth Assessment Report of the Intergovernmental Panel on Climate Change*, Stocker TF, Qin D, Plattner G-K, Tignor M, Allen SK, Boschung J, Nauels A, Xia Y, Bex V, Midgley PM (eds). Cambridge University Press: Cambridge, UK and New York, NY.

Diaz HF, Kiladis GN. 1992. Atmospheric teleconnections associated with the extreme phases of the Southern Oscillation. In *El Niño: Historical and Paleoclimatic Aspects of the Southern Oscillation*, Diaz HF, Markgraf V (eds). Cambridge University Press: Cambridge, UK, 7–28.

Diaz HF, Markgraf V. 2000. *El Niño and the Southern Oscillation: Multiscale Variability and Global and Regional Impacts*. Cambridge University Press: Cambridge, UK 496 pp.

Diaz HF, Hoerling MP, Eischeid JK. 2001. ENSO variability, teleconnections and climate change. *Int. J. Climatol.* **21**: 1845–1862.

DiNezio PN, Clement AC, Vecchi GA, Soden BJ, Kirtman BP. 2009. Climate response of the equatorial Pacific to global warming. *J. Clim.* **22**: 4873–4892.

Easterling DR, Evans JL, Groisman PY, Karl TR, Kunkel KE, Ambenje P. 2000a. Observed variability and trends in extreme climate events: a brief review. *Bull. Am. Meteorol. Soc.* **81**: 417–425.

Easterling DR, Meehl GA, Parmesan C, Changnon SA, Karl TR, Mearns LO. 2000b. Climate extremes: observations, modeling, and impacts. *Science* **289**: 2068–2074.

Fu C, Diaz HF, Fan H. 1992. Variability in latent heat flux over the tropical Pacific in association with recent two ENSO events. *Adv. Atmos. Sci.* **9**: 351–358.

Gao C, Robock A, Ammann C. 2008. Volcanic forcing of climate over the past 1500 years: an improved ice core-based index for climate models. *J. Geophys. Res. Atmos.* **113**: 1–15.

Gent PR, Danabasoglu G, Donner LJ, Holland MM, Hunke EC, Jayne SR, Lawrence DM, Neale RB, Rasch PJ, Vertenstein M, Worley PH, Yang ZL, Zhang M. 2011. The Community Climate System Model version 4. *J. Clim.* **24**: 4973–4991.

Guilyardi E, Wittenberg A, Fedorov A, Collins M, Wang C, Capotondi A, van Oldenborgh G, Stockdale T. 2009. Understanding El Niño in ocean–atmosphere general circulation models – progress and challenges. *Bull. Am. Meteorol. Soc.* **90**: 325–340.

Guilyardi EA, Bellenger H, Collins M, Ferrett S, Cai W, Wittenberg A. 2012. A first look at ENSO in CMIP5. *CLIVAR Exchange* **58**(1): 29–32.

Hansen J, Sato M, Ruedy R, Lo K, Lea DW, Medina-Elizade M. 2006. Global temperature change. *Proc. Natl. Acad. Sci. U.S.A.* **103**: 14288–14293.

Hartmann DL, AMG KT, Rusticucci M, Alexander LV, Brönnimann S, Charabi Y, Dentener FJ, Dlugokencky EJ, Easterling DR, Kaplan A, Soden BJ, Thorne PW, Wild M, Zhai PM. 2013. Observations: atmosphere and surface. In *Climate Change 2013: The Physical Science Basis. Contribution of Working Group I to the Fifth Assessment Report of the Intergovernmental Panel on Climate Change*, Stocker TF, Qin D, Plattner G-K, Tignor M, Allen SK, Boschung J, Nauels A, Xia Y, Bex V, Midgley PM (eds). Cambridge University Press: Cambridge, UK.

He C, Zhou T. 2015. Responses of the western North Pacific subtropical high to global warming under RCP4.5 and RCP8.5 scenarios projected by 33 CMIP5 models: the dominance of tropical Indian Ocean – tropical western Pacific SST gradient. *J. Clim.* **28**: 365–380.

Held IM, Soden BJ. 2006. Robust responses of the hydrological cycle to global warming. *J. Clim.* **19**: 5686–5699.

Knutson TR, Manabe S. 1995. Time-mean response over the tropical Pacific due to increased CO_2 in a coupled ocean–atmosphere model. *J. Clim.* **8**: 2181–2199.

Kunkel KE, Angel JR. 1999. Relationship of ENSO to snowfall and related cyclone activity in the contiguous United States. *J. Geophys. Res.* **104**(D16): 19425–19434.

Liu Z, Vavrus S, He F, Wen N, Zhong Y. 2005. Rethinking tropical ocean response to global warming: the enhanced equatorial warming. *J. Clim.* **18**: 4684–4700.

Liu J, Wang B, Cane MA, Yim S-Y, Lee J-Y. 2013. Divergent global precipitation changes induced by natural versus anthropogenic forcing. *Nature* **493**: 656–659.

Ma S, Zhou T. 2016. Robust strengthening and westward shift of the tropical Pacific Walker circulation during 1979–2012: a comparison of 7 sets of reanalysis data and 26 CMIP5 models. *J. Clim.* **29**: 3097–3118.

MacFarling Meure C, Etheridge D, Trudinger C, Steele P, Langenfelds R, van Ommen T, Smith A, Elkins J. 2006. Law Dome CO_2, CH_4 and N_2O ice core records extended to 2000 years BP. *Geophys. Res. Lett.* **33**: 1–4.

Mann ME, Cane MA, Zebiak SE, Clement A. 2005. Volcanic and solar forcing of the tropical Pacific over the past 1000 years. *J. Clim.* **18**: 447–456.

Meehl GA, Washington WM. 1996. El Niño-like climate change in a model with increased atmospheric CO_2 concentrations. *Nature* **382**: 56–60.

Meehl GA, Collins WD, Boville BA, Kiehl JT, Wigley TML, Arblaster JM. 2000. Response of the NCAR climate system model to increased CO_2 and the role of physical process. *J. Clim.* **13**: 1879–1898.

Meehl GA, Stocker TF, Collins WD, Friedlingstein P, Gaye AT, Gregory JM, Kitoh A, Knutti R, Murphy JM, Noda A, Raper SCB, Watterson IG, Weaver AJ, Zhao Z-C. 2007. Global climate projections. In *Climate Change 2007*: *The Physical Science Basis. Contribution of Working Group I to the Fourth Assessment Report of the Intergovernmental Panel on Climate Change*, Solomon S, Qin D, Manning M, Chen Z, Marquis M, Averyt KB, Tignor M, Miller HL (eds). Cambridge University Press: Cambridge, UK and New York, NY.

Neale RB, Richter J, Park S, Lauritzen PH, Vavrus SJ, Rasch PJ, Zhang M. 2013. The mean climate of the Community Atmosphere Model (CAM4) in forced SST and fully coupled experiments. *J. Clim.* **26**: 5150–5168.

Ning L, Bradley RS. 2014. Winter precipitation variability and corresponding teleconnections over the northeastern United States. *J. Geophys. Res. Atmos.* **119**: 7931–7945. https://doi.org/10.1002/2014JD021591.

Ning L, Bradley RS. 2015a. Winter climate extremes over the northeastern United States and southeastern Canada and teleconnections with large-scale modes of climate variability. *J. Clim.* **28**: 2475–2493. https://doi.org/10.1175/JCLI-D-13-00750.1.

Ning L, Bradley RS. 2015b. Influence of eastern Pacific and central Pacific El Niño events on winter climate extremes over the eastern and central United State. *Int. J. Climatol.* **35**: 4756–4770. https://doi.org/10.1002/joc.4321.

Seager R, Murtugudde R. 1997. Ocean dynamics, thermocline adjustment and regulation of tropical SST. *J. Clim.* **10**: 521–534.

Seager R, Zebiak SE, Cane MA. 1988. A model of the tropical Pacific sea surface temperature climatology. *J. Geophys. Res.* **93**: 1265–1280.

Shapiro AI, Schmutz W, Rozanov E, Schoell M, Haberreiter M, Shapiro AV, Nyeki S. 2011. A new approach to the long-term reconstruction of the solar irradiance leads to large historical solar forcing. *Astron. Astrophys.* **529**: A67.

Timmermann A, Oberhuber J, Bacher A, Esch M, Latif M, Roechner E. 1999. Increased El Niño frequency in a climate model forced by future greenhouse warming. *Nature* **398**: 694–697.

Trenberth KE, Jones PD, Ambenje P, Bojariu R, Easterling D, Klein Tank A, Parker D, Rahimzadeh F, Renwick JA, Rusticucci M, Soden B, Zhai P. 2007. Observations: surface and atmospheric climate change. In *Climate Change 2007*: *The Physical Science Basis. Contribution of Working Group I to the Fourth Assessment Report of the Intergovernmental Panel on Climate Change*, Solomon S, Qin D, Manning M, Chen Z, Marquis M, Averyt KB, Tignor M, Miller HL (eds). Cambridge University Press: Cambridge, UK and New York, NY.

Van Oldenborgh GJ, Philip SY, Collins M. 2005. El Niño in a changing climate: a multi-model study. *Ocean Sci.* **1**: 81–95.

Vecchi GA, Soden BJ. 2007. Global warming and the weakening of the tropical circulation. *J. Clim.* **20**: 4316–4340.

Vecchi GA, Soden BJ, Wittenberg AT, Held IM, Leetmaa A, Harrison MJ. 2006. Weakening of tropical Pacific atmospheric circulation due to anthropogenic forcing. *Nature* **441**: 73–76.

Vecchi GA, Clement A, Soden BJ. 2008. Examining the tropical Pacific's response to global warming. *Eos Trans. AGU* **89**: 81–83. https://doi.org/10.1029/2008EO090002.

Wang Z, Li Y, Liu B, Liu J. 2015. Global climate internal variability in a 2000-year control simulation control simulation with Community Earth System Model (CESM). *Chin. Geogr. Sci.* **25**: 263–273.

Weare BC. 2013. El Niño teleconnections in CMIP5. *Clim. Dyn.* **41**: 2165–2177.

Xie S, Deser C, Vecchi GA, Ma J, Teng H, Wittenberg AT. 2010. Global warming pattern formation: sea surface temperature and rainfall. *J. Clim.* **23**: 966–986.

Yu J-Y, Zou Y, Kim ST, Lee T. 2012. The changing impact of El Niño on US winter temperatures. *Geophys. Res. Lett.* **39**: L15702. https://doi.org/10.1029/2012GL052483.

Zhang M, Song H. 2006. Evidence of deceleration of atmospheric vertical overturning circulation over the tropical Pacific. *Geophys. Res. Lett.* **33**: L12701. https://doi.org/10.1029/2006GL025942.

Zou Y, Yu J-Y, Lee T, Lu M-M, Kim ST. 2014. CMIP5 model simulations of the impacts of the two types of El Niño on the U.S. winter temperature. *J. Geophys. Res. Atmos.* **119**: 3076–3092. https://doi.org/10.1002/2013JD021064.

